Research Square

Preprints are preliminary reports that have not undergone peer review.
They should not be considered conclusive, used to inform clinical practice,
or referenced by the media as validated information.

Exploration of potential mechanisms and key genes associated with stress granules in immunoglobulin A nephropathy based on transcriptome and experimental validation

Guzailinuer Sailaiajimu

guzelnue0908@163.com

the First Affiliated Hospital of Xinjiang Medical University

Research Article

Keywords: Bioinformatics, Immunoglobulin A nephropathy, Key genes, Stress granules, Transcriptome sequencing

Posted Date: September 24th, 2026

DOI: https://doi.org/10.21203/rs.3.rs-10599847/v1

License: This work is licensed under a Creative Commons Attribution 4.0 International License.
Read Full License

Additional Declarations: No competing interests reported.

Abstract

Background

Stress granules (SGs) are involved in immunoglobulin A nephropathy (IgAN) pathogenic pathogenesis. This study aimed to identify SGs-related key genes in IgAN and explore their underlying mechanisms and therapeutic potential.

Methods

After IgAN modeling in rats, RNA sequencing was conducted to obtain their transcriptome data, and human SGs-related genes (SGs-RGs) were downloaded from public databases. Subsequently, differentially expressed genes (DEGs) were identified, and candidate genes were obtained by intersecting with rat SGs-RGs (converted from human SGs-RGs through homologous mapping). Key genes were finally determined through the protein-protein interaction network and the MCODE plug-in. Meanwhile, we performed in-depth analyses—including functional enrichment, drug prediction, molecular docking, and molecular dynamics simulations—on the hub genes. In addition, experimental verification of the key genes was additionally performed.

Results

A total of 53 candidate genes were identified. After multiple rounds of screening, Jun, Ers1, Fos, Jun, and Myc were finally determined as key genes. These genes (except Esr1) showed positive correlations (correlation > 0.30) and functional similarity (score > 0.50), and were enriched in pathways such as ribosome signaling pathway. After cross-species homologous mapping, multiple human key genes (Jun, Ers1, Fos, Jun, and Myc) were targeted by the same transcription factor or the same non-coding RNA and exhibited a shared regulatory targeting pattern. In addition, the predicted drug daidzein showed good binding activity with the corresponding proteins of key genes (docking score < -5 kcal/mol); the optimal binding system was formed by ESR1 and daidzein, while the most stable and rigid binding system was formed by PTGS2 and daidzein. Moreover, these bioinformatics findings were further verified experimental assays.

Conclusion

Jun, Ers1, Fos, Jun, and Myc were potential key genes associated with SGs in IgAN. Daidzein might target them to exert therapeutic effects, providing a reference for revealing SGs' role in IgAN.

1. Background

Immunoglobulin A nephropathy (IgAN) is a primary glomerular disorder defined by the mesangial deposition of IgA-dominant immune complexes and ranks among the most prevalent forms of primary chronic glomerulonephritis globally [1]. Clinically, IgAN presents with recurrent episodes of macroscopic or microscopic hematuria, often accompanied by proteinuria; a subset of patients may develop hypertension and progressive renal dysfunction, ultimately advancing to end-stage renal disease (ESRD) [2, 3]. Epidemiological investigations suggest that the progression of IgAN varies considerably, and roughly 20%-40% of patients develop ESRD within 10 to 20 years following diagnosis, imposing substantial medical and economic burdens on patients and society [4]. Current treatment strategies primarily include supportive care—such as blood pressure control and reduction of proteinuria level—and immunosuppressive therapy; however, specific targeted therapies are lacking, and some patients exhibit poor response to therapy [5–7]. Although aberrant glycosylation of IgA, immune complex deposition, and subsequent mesangial inflammation are well-recognized to contribute to IgAN pathogenesis [2], the underlying molecular regulatory mechanisms—particularly the key links between cellular stress responses and pathological injury—remain largely unexplored.

Stress granules (SGs) are dynamic cytoplasmic assemblies formed by RNA-binding proteins and mRNAs in response to cellular stressors, such as oxidative stress, hypoxia, or viral infection [8]. They serve to protect mRNAs from degradation, pause protein translation, and engage in signal transduction and adaptive stress responses, playing a critical role in maintaining cellular homeostasis under adverse conditions [9]. Evidence suggests that SGs are activated in various renal disorders, including acute kidney injury (AKI) and chronic diabetic nephropathy (DN), modulating stress responses, inflammatory cytokine release, and apoptosis, thereby influencing disease progression [10]. For instance, SG formation in acute kidney injury models mitigates tubular epithelial cell damage, whereas defective assembly or clearance exacerbates injury [11]. Despite these insights, research on SGs in IgAN remains extremely limited. Whether SGs influence mesangial cell stress responses, immune complex clearance, or inflammation during IgA deposition, and the role of SG-related key genes in IgAN pathogenesis, is not yet elucidated, highlighting a critical knowledge gap.

In this study, we leveraged rat transcriptomic sequencing data and bioinformatics approaches to identify key SG-related genes in IgAN. Functional enrichment analyses were conducted to clarify their roles in SG function and IgAN pathology, alongside the construction of molecular regulatory networks, drug prediction, molecular docking, and dynamic simulations. Key genes were further validated experimentally. Our findings fill a critical gap in understanding SG-associated mechanisms in IgAN, provide theoretical insights into novel pathogenic pathways, and lay a foundation for developing targeted therapies focused on SG-related genes.

2. Methods

2.1 Acquisition of the rat dataset

First, twelve 6-week-old specific pathogen-free female Sprague-Dawley rats were randomly allocated into a control group and a model group (n = 6 per group). After one week of acclimatization with confirmed negative urinary erythrocyte tests, the modeling procedure was initiated. The IgAN rat model was established in the model group using a combined immunization method, which consisted of oral gavage with bovine serum albumin (BSA) at 400 mg/kg every other day for 8 weeks, concurrent weekly subcutaneous injections of 0.1 ml of a 5:1 castor oil and CCl4 mixture on the back for 9 weeks along with intraperitoneal injections of 0.06 ml of the same mixture every two weeks during this period, and tail vein injections of 50 μg lipopolysaccharide at weeks 6 and 8. The control group received equivalent volumes of distilled water by gavage and saline via subcutaneous, intraperitoneal, and tail vein injections on the same schedule. Following the modeling period, sequencing was performed on 6 pairs of tissue samples collected from the model and control groups, respectively.The detailed experimental process was performed as follows: Total RNA extraction was completed using Trizol reagent, which was sourced from Invitrogen (Carlsbad, CA, USA), the quality and concentration of total RNA were evaluated using a Bioanalyzer 2100 (Agilent, CA, USA) to ensure that the RNA samples met the requirements for downstream experiments, with a concentration surpassing 50 ng/μL, a RIN (RNA Integrity Number) value exceeding 7.0, an OD260/280 ratio higher than 1.8, and total RNA amount exceeding 1 μg. Two rounds of mRNA purification from total RNA were performed with Dynabeads Oligo (dT) [Catalog Number: 25-61005; Thermo Fisher Scientific, USA]. The purified mRNA was incubated at 94°C for 5–7 minutes with the NEBNext® Magnesium RNA Fragmentation Module (Catalog Number: E6150S, New England Biolabs, USA) to fully fragment the mRNA into short fragments. These fragmented RNA fragments were reverse-transcribed into cDNA using Invitrogen SuperScript™ II Reverse Transcriptase (Catalog Number: 1896649, Carlsbad, CA, USA). Subsequently, double-stranded DNA was synthesized with E. coli DNA polymerase I (provided by New England Biolabs [NEB], Catalog Number: m0209, USA) and RNase H (also sourced from NEB, Catalog Number: m0297, USA). After this step, dUTP Solution (Thermo Fisher Scientific, Catalog Number: R0133, California, USA) was added, and end repair was then conducted. An adenine (A) base was appended to the blunt end of each individual DNA fragment. resulting in A-overhangs at both ends of the DNA fragments to match the adapters with T-overhangs. After adapter ligation, size selection of the DNA fragments was conducted with the use of magnetic beads. Further, Treatment of U-labeled double-stranded DNA was performed with UDG enzyme (New England Biolabs [NEB], Catalog Number: m0280, Massachusetts, USA), after which polymerase chain reaction (PCR) amplification was performed. Finally, a library featuring DNA fragments sized at 300 bp ± 50 bp was successfully acquired. Ultimately, following standard protocols, paired-end sequencing was carried out on the Illumina Novaseq™ 6000 platform (LC-Bio Technology Co., Ltd., Hangzhou, China) using a PE150 sequencing mode (150 bp per end read length). To guarantee high-quality and pure reads, quality control (QC) was conducted using fastp (available at https://github.com/OpenGene/fastp) with the default parameters. This process involved removing adapter sequences, duplicate sequences, and low-quality sequences to generate clean data. Next, the quality-controlled sequencing data were mapped to the human genome (Homo sapiens, GRCh38) using HISAT2 (accessible at https://ccb.jhu.edu/software/hisat2/), with the output format set to bam. In addition, StringTie (https://ccb.jhu.edu/software/stringtie/) was employed to compute the FPKM (Fragments Per Kilobase

of exon per Million mapped fragments) values corresponding to each gene. The above RNA sequencing data were recorded as the rat dataset.

2.2 Acquisition of stress granule (SGs)-related genes

According to the literature [12], 844 human genes related to SGs (human SGs-related genes, human SGs-RGs) were obtained by searching the GeneCards:® The Human Gene Database (available at https://www.genecards.org) was searched using the keyword "stress granules" and specifying that the relevance score should be greater than 4 (**Additional file 1**).

2.3 Acquisition of key genes

The "DESeq2" package (v 1.38.0) [13] was used to identify DEGs (differentially expressed genes) between the model and control groups in the rat dataset, with filtering conditions: $|\log_2 \text{FoldChange (FC)}| > 0.5$ and $p < 0.05$. A volcano plot of the DEGs was constructed using "ggplot2" (v 3.4.4) [14], with the top 5 upregulated and downregulated genes exhibiting the largest $|\log_2 FC|$ changes labeled. In addition, a heatmap of these labeled genes was created using "ComplexHeatmap" (v 2.18.0) [15].

To screen candidate genes related to IgAN and SGs, 844 human SGs-RGs were first converted into rat SGs-RGs (after deduplication) through cross-species homologous gene mapping using the getLDS() function in "biomaRt" (v 2.54.0) [16]combined with the Ensembl database (https://www.ensembl.org/). Then, intersection analysis of DEGs and rat SGs-RGs was performed using "ggvenn" (v 0.1.9) [17] to obtain candidate genes.

Subsequently, to examine the potential biological functions and signaling pathways linked to the candidate genes, enrichment analyses of GO (Gene Ontology) and KEGG (Kyoto Encyclopedia of Genes and Genomes) were carried out using "clusterProfiler" (v 4.10.0) [18] with a threshold of $p < 0.05$, and the results of several pathways enriched with the highest number of genes were presented.

Meanwhile, to examine how the candidate genes interact with each other at the protein level, the candidate genes were uploaded to the Search Tool for the Retrieval of Interacting Genes/Proteins (STRING) database (available at http://string-db.org), and a threshold of 0.7 was set to construct a protein-protein interaction (PPI) network. The top 10 genes ranked by Degree (sorted from high to low) were highlighted in yellow. Furthermore, the "MCODE" plugin in Cytoscape (v 3.10.3) [19] was utilized to identify key modules within the PPI network. Key sub-modules with an MCODE score > 3 and no fewer than 5 nodes were screened, and the node genes within these sub-modules were identified as hub genes for subsequent analyses.

2.4 Correlation analysis of key genes

Next, to examine biological pathways related to hub genes in IgAN, the "psych" tool (v 2.2.9 ADDIN EN.CITE) [20] was utilized to determine Spearman correlation coefficients between hub genes and other genes in the rat dataset samples, and genes were ranked in descending order based on the correlation coefficients. Meanwhile, based on the KEGG rat dataset, Gene Set Enrichment Analysis (GSEA) was

performed using the "clusterProfiler" (v 4.10.0). The screening criteria were (|Normalized Enrichment Score (NES)| > 1, p < 0.05), and the top 10 results were presented sorted by p value in ascending order. Furthermore, to further reveal the differences in pathways of key genes during the IgAN process, still based on the rat dataset and KEGG rat dataset, Gene Set Variation Analysis (GSVA) was first performed on the model group and control group samples using the "GSVA" (v 1.46.0) [21] to calculate pathway scores. Then, differences in pathway scores between the two groups were compared using the Wilcoxon rank-sum test, and the top 5 upregulated and downregulated pathways were selected and presented sorted by t value in descending order (|t| > 2, p < 0.05).

To quantify the degree of association between key genes, correlation analysis was performed using "corrplot" (v 0.92 ADDIN EN.CITE) [22] with the criteria of |correlation (cor)| > 0.30 and p < 0.0001. Meanwhile, to explore whether key genes had functional similarity, the "GOSemSim" (v 2.24.0) [23] was employed to compute the GO semantic similarity among key genes. Generally, a functional similarity score > 0.50 indicated high functional similarity between genes.

To investigate the molecular regulatory mechanisms that underlie hub genes, the key genes were converted into human key genes based on the Ensembl database using the getLDS function in "biomaRt" (v 2.54.0). Transcription factors (TFs) that can interact with human hub genes were predicted using the NetworkAnalyst database (accessible at https://www.networkanalyst.ca/). Additionally, microRNAs (miRNAs) and long non-coding RNAs (lncRNAs) that can interact with human key genes were predicted using the get_multimir function of "multiMiR" (v 1.20.0 ADDIN EN.CITE) [24]. On this basis, TF-mRNA and lncRNA-miRNA-mRNA regulatory networks were established.

To further screen for potential therapeutic agents targeting IgAN, the "enrichR" (v 3.2 ADDIN EN.CITE) [25] was used to predict potential drugs interacting with key genes, and partial results (top 10) were presented based on the Combined.Score ranking. On this basis, key potential drugs with higher Odds.Ratio and Combined.Score rankings and related to IgAN were further screened for molecular docking. Specifically, the protein structures of hub genes were retrieved from the Uniprot database (accessible at https://www.uniprot.org/), whereas the three-dimensional structures of key potential drugs were acquired from the PubChem database, which is available at https://pubchem.ncbi.nlm.nih.gov/. These two types of structures were imported into the online tool CB-DOCK2 (https://cadd.labshare.cn/cb-dock2/) for docking. Generally, a docking score of less than − 5.0 kcal/mol was regarded as an indicator of favorable binding activity.

Furthermore, to verify the rationality and reliability of the docking results, the target protein sequences of rat species were retrieved and screened from the National Center for Biotechnology Information database (https://www.ncbi.nlm.nih.gov/), and GROMACS software (v 2024.2 ADDIN EN.CITE) [26] was used to carry out 100 ns molecular dynamics simulations. In the generation of parameters and topology files, the AMBER14SB force field was used to process proteins, and the General Amber Force Field (GAFF) was used to process small molecule ligands. In the system construction stage, -eriodic boundary conditions were applied, the size of the simulation box was adjusted optimally, and the box was filled

with water molecules. To ensure the system's electrical neutrality, some solvent water molecules were exchanged with Na^+ and Cl^- at a concentration of 0.15 mol/L. Once the entire system underwent energy minimization via the steepest descent method, pre-equilibration was performed in two steps. The first step used the NVT ensemble (constant particles, volume, temperature) for 100 ps at 300 K to stabilize system temperature, and the second step employed the NPT ensemble (constant particles, pressure, temperature) for 100 ps at 1 bar to stabilize system pressure, laying a stable foundation for subsequent simulations. After completion of equilibration, the system entered the production simulation stage. To comprehensively assess the structural changes and interaction features of the protein-ligand complex, key parameters were calculated, including Root Mean Square Deviation (RMSD) and Root Mean Square Fluctuation (RMSF) of protein residues, total system energy, and the number of hydrogen bonds.

2.5 Reverse transcription-quantitative polymerase chain reaction (RT-qPCR)

Animals were obtained from Sibeifu Biotechnology Co., Ltd. At the experimental endpoint prior to tissue collection, rats were deeply anesthetized with isoflurane inhalation. Briefly, rats were placed in an anesthesia induction chamber and anesthetized with 3%–5% isoflurane until loss of consciousness and disappearance of the righting reflex. They were then transferred to the operating table, and anesthesia was maintained via a nose cone with 1.5%–3% isoflurane. Anesthetic depth was dynamically assessed based on respiratory rate, muscle tone, and the toe-pinch reflex, and the isoflurane concentration was adjusted accordingly. Once the toe-pinch reflex was absent, confirming deep anesthesia, rats were euthanized by exsanguination followed by cervical dislocation to confirm death before sample collection.

First, total RNA was isolated from five pairs of rat tissue samples, containing 5 kidney tissue samples from the model group and 5 from the control group) with Trizol reagent (Vazyme, China), and RNA concentration was determined using a NanoPhotometer N50. cDNA was synthesized with the HP All-in-one qRT Master Mix II RT203-Ver.1 kit (provided by Younggen, China). Quantitative PCR was conducted using the CFX system (Bio-Rad, USA). To ensure reliable results, the experiment was repeated three times, and the relative expression levels of hub genes were calculated using the $2^{-\Delta\Delta Ct}$ method. The results were normalized against the internal reference gene GAPDH. Experimental data were analyzed using GraphPad Prism 10 [27]. The corresponding primer sequences are presented in **Additional file 2**. Differences between the two groups were assessed using Student's t-test.

2.6 Statistical analysis

All analyses were carried out in R (v 4.2.2), with statistical significance defined as a p-value < 0.05. Cohort comparisons utilized the Wilcoxon rank-sum test. For RT-qPCR analyses, differences within groups were assessed using the Student's t-test.

3. Results

3.1 Acquisition of key genes related to SGs in IgAN

The present study aimed to systematically identify key genes closely associated with the formation and function of SGs in IgAN. To this end, we integrated the transcriptome data of a rat IgAN model with a human SGs-related gene database, and screened candidate genes through differential expression analysis and protein-protein interaction network analysis. This strategy drew on the method used by Liu et al. to construct a prognostic model based on SGs in colorectal cancer, highlighting the feasibility and reliability of cross-species homologous mapping in disease mechanism research [12]. Through this design, we expected to reveal the molecular basis of SGs in IgAN and provide targets for subsequent functional verification. Based on the above analysis process, we successfully screened out 968 DEGs from the rat datase ($|\log_2 FC| > 0.5$, $p < 0.05$). Among them, relative to the control group, the model group had 257 upregulated genes and 711 downregulated genes (**Additional file 3**). The volcano plot of DEGs and the heatmap of labeled DEGs are presented in Figs. 1a-b. Subsequently, after cross-species homologous gene conversion, 864 rat SGs-RGs were obtained, and 53 candidate genes were identified through intersection analysis (Fig. 1c; **Additional file 4**). To further analyze the biological significance of the candidate genes, we conducted GO and KEGG enrichment analyses on them ($p < 0.05$) .The findings indicated that a total of 1,355 functional terms were acquired from GO enrichment analysis, including 1,221 terms in Biological Process (BP), 68 terms in Cellular Component (CC), and 66 terms in Molecular Function (MF). These terms involved multiple important functions, such as response to hypoxia, response to decreased oxygen levels, transcription regulator complex, cytoplasmic ribonucleoprotein granule, RNA polymerase II-specific DNA-binding activity of transcription activators, and general DNA-binding activity of transcription activators (**Additional file 5**; Fig. 1d). KEGG enrichment analysis covered 90 pathways, including apelin signaling pathway, mitogen-activated protein kinase (MAPK) signaling pathway, interleukin (IL)-17 signaling pathway, and T cell receptor signaling pathway (**Additional file 6**; Fig. 1e).In addition, the PPI network constructed based on candidate genes (Fig. 1f) showed 37 interaction relationships (after removing 30 isolated targets). It was worth noting that multiple genes had formed relatively tight interaction modules, among which genes such as Jun, Fos, and Esr1 had constituted the core of the module. The top 10 genes were Jun, Fos, Esr1, Tlr4, Ptgs2, Myc, Gsk3b, Ppargc1a, Atf3, and Mapk8 (Fig. 1g). The node genes in the further identified key sub-modules, namely key genes, were Jun, Fos, Esr1, Ptgs2, and Myc (score = 5) (Fig. 1h).

3.2 Key genes analysis of correlation, functional similarity, and pathway enrichment

To gain an in-depth understanding of the mechanism underlying the synergistic action of key genes in IgAN, we conducted correlation analysis, functional similarity assessment, and pathway enrichment analysis. This design was based on the study by Zhou et al., who verified the expression patterns of key genes in IgAN patients and emphasized the importance of multi-gene co-expression networks in disease classification [28]. Through GSEA and GSVA, we further revealed the enrichment of these genes in pathways such as the MAPK pathway and ribosome pathway, providing system-level evidence for

understanding their synergistic regulation of the IgAN progression. First, correlation analysis of hub genes (Fig. 2a) revealed significant positive correlations among certain hub genes. Among them, the most significant positive correlation occurred between Fos and Jun (cor = 0.91, $p < 0.001$), while the correlation between Myc and Fos ranked second (cor = 0.84, $p < 0.001$). Functional similarity analysis showed that the functional similarity scores of all 5 hub genes exceeded 0.5, which implies that these genes may exhibit shared functional mechanisms when involved in relevant biological processes. Among them, the Jun gene had a relatively high functional similarity score, which indicates that it may exert a more crucial function among these key genes (Fig. 2b).

Subsequently, GSEA was used to explore potential signaling pathways related to key genes ($|NES| > 1$, $p < 0.05$). The results showed that Esr1, Fos, Jun, Myc, and Ptgs2 were enriched in 55, 19, 24, 21, and 45 pathways, respectively (**Additional file 7–11**). Specifically, Esr1 was significantly enriched in pathways including ribosome and focal adhesion, and endocytosis; Fos was significantly enriched in pathways including ribosome, MAPK signaling pathway, and Extracellular Matrix (ECM)-receptor interaction; Jun was significantly enriched in pathways such as ECM-receptor interaction, focal adhesion, and MAPK signaling pathway; Myc was significantly enriched in pathways including ribosome, MAPK signaling pathway, and ECM-receptor interaction; Ptgs2 was significantly enriched in pathways such as MAPK signaling pathway, ribosome, and circadian rhythm-mammal (Figs. 2c-g). The aforementioned findings indicated that key genes may synergistically contribute to the onset and progression of IgAN, and SGs-related cellular stress adaptation processes through cross-regulation of pathways, involving multiple aspects such as stress response, immune inflammation, maintenance of renal structure, and metabolic rhythm. Meanwhile, when compared with the control group, the model group displayed 14 pathways with significant activation and 17 pathways with marked inhibition. For example, pathways such as folate biosynthesis, protein export, and proteasome were significantly activated ($t > 2$, $p < 0.05$), while pathways including dorso ventral axis formation, circadian rhythm mammal, and taste transduction were significantly inhibited ($t < -2$, $p < 0.05$) (**Additional file 12**; Fig. 2h).

3.3 Key genes analysis of molecular regulation, drug prediction, molecular docking, and molecular dynamics simulation

To explore the regulatory mechanisms of key genes and their potential as drug targets, we constructed TF-mRNA and lncRNA-miRNA-mRNA regulatory networks, and conducted drug prediction and molecular docking simulations. This approach drew on the research idea of Noor et al., who constructed a miRNA-mRNA regulatory network in IgAN, highlighting the crucial role of non-coding RNAs in disease regulation [29]. Furthermore, we evaluated the stability of drug-protein binding through molecular dynamics simulations, which provides a theoretical basis for subsequent experimental verification and drug development. Next, an in-depth analysis of the regulatory mechanisms of key genes was performed. The results showed that 73 TFs, 8 miRNAs, and 71 lncRNAs were predicted for JUN; 3 TFs were predicted for PTGS2; 62 TFs, 32 miRNAs, and 248 lncRNAs were predicted for MYC; 52 TFs, 14 miRNAs, and 159 lncRNAs were predicted for FOS; and 1 TF, 9 miRNAs, and 85 lncRNAs were predicted for ESR1

(**Additional file 13–14**). Based on the above results, the constructed regulatory networks were shown in Figs. 3a-b. It was worth noting that multiple human key genes could be targeted by the same transcription factor or the same non-coding RNA (e.g., miRNA, lncRNA) and exhibited a shared targeting pattern. This laid a molecular association foundation for analyzing their regulatory mechanisms in disease-related processes.

Based on predictions, a total of 1,630 potential drugs that might interact with the 5 key genes were identified (**Additional file 15**), among which the top 10 ranked by Combined Score were shown in Table 1. Further screening was conducted to select daidzein, a drug with high rankings in both Odds. Ratio and Combined.Score and associated with IgAN, for molecular docking. The specific details were presented in Table 2 and Fig. 3c. Data showed that the docking energy between Jun and daidzein was − 5 kcal/mol; the docking energy between Fos and daidzein was − 5.5 kcal/mol; the docking energy between each of Esr1 and daidzein was − 8.8 kcal/mol; the docking energy between each of Ptgs2 and daidzein was − 8.5 kcal/mol; and the docking energy between Myc and daidzein was − 5.9 kcal/mol. This indicated that all proteins encoded by key genes had good binding activity with daidzein, suggesting that daidzein had the potential to become a potential drug for regulating the functions of key genes, and provided preliminary molecular docking evidence for the subsequent exploration of intervention strategies targeting these genes.

In addition, there were differences in the binding modes between the proteins encoded by the key genes and daidzein, which were specifically manifested in the following aspects: During the binding process with daidzein, Esr1 and Ptgs2 showed lower RMSD values and converged rapidly in the early stage of the simulation, indicating that these proteins had strong binding ability and high conformational rigidity with daidzein. In contrast, Fos, Jun, and Myc underwent more drastic conformational adjustments in the early stage of the simulation; although they tended to stabilize in the later stage, their absolute RMSD values were higher, showing stronger structural flexibility and dynamic characteristics, which might be related to their protein functions and the properties of their binding sites (Fig. 3d). When combined with daidzein, the structure of Ptgs2 is the most stable and exhibits a more extensive flexible region; the high volatility of Fos, Jun, and Myc was mainly concentrated at the N-terminus (Fig. 3e). In terms of energy changes, Fos had the lowest energy with small fluctuations when binding to daidzein, showing the strongest thermodynamic tendency for spontaneity and binding stability; Ptgs2, Jun, and Myc had similar energy levels, which were in the medium range, with moderate thermodynamic stability; although the energy change of Esr1 was stable, its overall energy was higher, resulting in relatively weaker binding stability (Fig. 3f). In terms of hydrogen bond interactions, the number of hydrogen bonds between Ptgs2 and daidzein reached a high peak with significant dynamic changes, indicating that hydrogen bonds played a key role in their binding process and reflected a flexible binding mode; the underlying yellow signal in the hydrogen bond map of Ptgs2 persisted, suggesting that its core hydrogen bond skeleton was stable, and the stability of the system might depend more on such basic interactions; Esr1, Fos, Jun, and Myc contributed fewer hydrogen bonds, and their binding driving force might mainly come from non-hydrogen bond interactions (e.g., hydrophobic interactions, van der Waals forces, etc.) (Fig. 3g). In summary, Ptgs2

and daidzein formed the optimal binding system, while Ptgs2 and daidzein formed the most stable and rigid binding system.

Table 1
Drug prediction results (taking the top 10 ranked by Combined.Score as an example)

Term	P.value	Combined.Score	Genes
IN1152	1.46930528687116e-12	2712634.8	Jun;Myc;Fos;Ptgs2;Esr1
daidzein	9.53553159836730e-12	2521485.855	Jun;Myc;Fos;Ptgs2;Esr1
cinnamaldehyde	3.59586771669705e-11	2385024.933	Jun;Myc;Fos;Ptgs2;Esr1
1-chloro-2,4-dinitrobenzene	2.48876804372604e-10	2184648.294	Jun;Myc;Fos;Ptgs2;Esr1
PD 98059	3.71367729702839e-10	2142937.721	Jun;Myc;Fos;Ptgs2;Esr1
17-Ethynyl estradiol	7.8521225500113e-10	2064639.803	Jun;Myc;Fos;Ptgs2;Esr1
Fulvestrant	8.66378582235025e-10	2054326.53	Jun;Myc;Fos;Ptgs2;Esr1
N-Acetyl-L-cysteine	9.3902516864751e-10	2045879.652	Jun;Myc;Fos;Ptgs2;Esr1
Phorbol 12-myristate 13-acetate	8.04843139155802e-09	1818768.603	Jun;Myc;Fos;Ptgs2;Esr1
oxygen	1.21155439829644e-08	1775118.264	Jun;Myc;Fos;Ptgs2;Esr1

Table 2
Molecular docking results

Gene	Drug	CID	AlphaFoldDB ID	Energy
Jun	daidzein	5281708	AF-P17325-F1-v4	-5
Fos	daidzein	5281708	AF-P12841-F1-v4	-5.5
Esr1	daidzein	5281708	AF-P06211-F1-v4	-8.8
Ptgs2	daidzein	5281708	AF-P35355-F1-v4	-8.5
Myc	daidzein	5281708	AF-P09416-F1-v4	-5.9

3.4 RT-qPCR validation

To verify the reliability of the bioinformatics analysis results, we used RT-qPCR to detect the expression levels of key genes in the IgAN model group and the control group. This experimental design referenced

the strategy employed by Wang et al., who verified the expression of SGs-related genes in a renal ischemia-reperfusion injury model, and emphasized the necessity of experimental validation in bioinformatics research [30]. Supported by the experimental data, we further confirmed the expression trends of key genes in IgAN, which enhances the credibility and translational potential of this study. To validate the reliability of the bioinformatics findings, RT-qPCR experiments were performed. Results indicated that in comparison to the control group, the model group had significantly reduced expression levels of Jun, Fos, Ptgs2, and Myc ($p < 0.05$), among which the difference in Myc expression was the most significant ($p < 0.001$). It is worth mentioning that the expression level of Esr1 in the model group was slightly lower than in the control group, but there had been no statistical difference. This discrepancy might be due to variations in RNA integrity and purity resulting from differences in RNA extraction, storage conditions, or other experimental factors. In conclusion, the above results indicated that the data mining results were reliable and possessed potential research value (Fig. 4).

4. Discussion

A primary characteristic of IgA nephropathy is the deposition of galactose-deficient IgA1 (Gd-IgA1) within the glomerular mesangial region. These deposited Gd-IgA1 molecules form immune complexes with anti-glycan IgG or IgA antibodies, the complexes then activate inflammatory pathways, subsequently triggering glomerular inflammation and fibrosis, and eventually resulting in a poor prognosis [31]. However, due to the incomplete elucidation of its pathogenesis, there remains a lack of reliable biomarkers for early diagnosis. As a cellular stress adaptation mechanism, SGs have been documented to be linked to a range of diseases, encompassing kidney disorders and cancers [10, 32]. Studies have shown that renal ischemia-reperfusion induces SG formation in proximal tubular cells, and dismantling the key component of SG assembly-G3BP1, which disrupts SG assembly, thereby promoting apoptosis [30]. SGs participate in disease progression by modulating key processes such as cellular stress responses, inflammatory cytokine release, and apoptosis [10].

This research seeks to identify key genes and molecular pathways linked to both IgAN and SGs, utilizing bioinformatics approaches such as PPI networks, functional enrichment analysis, and molecular docking simulations. Through these methods, Jun, Fos, Esr1, Ptgs2, and Myc were identified as critical genes involved in the pathogenesis of SGs-related IgAN. At the same time, relevant studies were conducted on key genes concerning correlation/function similarity, functional enrichment, molecular regulatory network construction, drug prediction, molecular docking, molecular dynamics simulation, and experimental validation. The results indicated that these genes (excluding Esr1) exhibited a positive correlation (correlation coefficient > 0.3) and demonstrated functional similarity (functional similarity score higher than 0.5), collectively enriching in pathways such as MAPK signaling pathway and ribosome pathway. More importantly, after performing interspecies homology mapping, several key human genes (including JUN, FOS, ESR1, PTGS2, and MYC) were found to be targeted by the same transcription factor or the same non-coding RNA (such as miRNA and lncRNA), exhibiting a shared regulatory pattern. In addition, the predicted drug daidzein demonstrated good binding activity with the proteins encoded by the corresponding key genes (docking score < -5 kcal/mol); specifically, Esr1 formed the optimal binding

system with daidzein, while Ptgs2 and daidzein formed the most stable and rigid binding conformation. The experimental results further validated the reliability of the bioinformatics analysis [28, 29].

The key genes identified in this study do not act in isolation, but rather through the coordinated regulation of a complete pathological network composed of "cellular stress response-immune-inflammatory activation-extracellular matrix (ECM) remodeling" ,collectively driving the progression of IgAN. This network also highlights the role of SGs as molecular hubs in linking initial stress signals to terminal renal injury. First, the cellular stress response serves as the initiating link in the pathological cascade. The enrichment analysis in this study indicates that key genes are significantly associated with hypoxic responses and the MAPK signaling pathway. In IgAN, the glomerular hypoxic microenvironment and oxidative stress induced by abnormal IgA deposition constitute the core biological stress faced by mesangial cells [33, 34]. Such stress not only directly damages cellular structures but also acts as a classical trigger for SG formation, initiating a series of adaptive and pathogenic cellular responses [35]. Next, stress signals are rapidly converted into immune-inflammatory activation. The enrichment of key genes in the IL-17 signaling pathway is critical. As a potent pro-inflammatory factor, IL-17 directly stimulates mesangial cell proliferation and secretion of various inflammatory mediators, significantly amplifying local renal inflammatory responses [36, 37]. Importantly, the inflammatory signals themselves can also act as stress sources, feedback-regulating SG assembly and disassembly, thereby forming a "stress-SGs-inflammation" positive feedback loop, which may represent an important mechanism for the persistence of chronic inflammation in IgAN. Ultimately, sustained inflammation and stress jointly drive ECM remodeling, forming the direct pathological basis for renal fibrosis. The enrichment of key genes in the ECM-receptor interaction pathway suggests their direct involvement in regulating the metabolism of matrix components such as collagen. In IgAN, activated mesangial cells lead to excessive ECM deposition, ultimately triggering glomerulosclerosis [38].

In SGs-related IgAN, the genes Jun Proto-Oncogene (JUN), FBJ murine osteosarcoma viral oncogene homolog (FOS), Myelocytomatosis Viral Oncogene Homolog (MYC), Estrogen Receptor 1 (ESR1), and Prostaglandin-Endoperoxide Synthase 2 (PTGS2) collaboratively regulate multiple critical pathways. They are involved in processes such as cellular stress adaptation, immune inflammation, maintenance of renal structure, and metabolic rhythms, collectively influencing the occurrence and progression of the disease. This highlights their significant pathological relevance and potential for application.

The JUN gene encodes the Jun protein, which serves as a core component of the activator protein-1 (AP-1) transcription factor family. It can form heterodimers with Fos proteins and regulates transcription by binding to target gene promoters, participating extensively in cell proliferation, stress responses, and inflammation regulation [39–41]. In IgAN, JUN was strongly positively correlated with Fos (cor = 0.91, $p < 0.05$), and the functional similarity score was relatively high (> 0.7), indicating it serves a core function in the hub gene network. It is significantly enriched in ECM-receptor interactions, focal adhesions, and MAPK signaling pathways, which are closely related to renal structural stability and inflammation activation [42]. Moreover, the expression of JUN is significantly reduced in the model group ($p < 0.05$), and this reduction potentially impairing cell stress adaptation by down regulating these pathways and

exacerbating renal inflammation and structural damage [43]. Therefore, JUN could serve as a potential key gene for assessing IgAN progression, and targeting the activation of JUN activation may restore pathway function and alleviate pathological damage.

The FOS gene encodes the Fos protein, which collaborates with the Jun protein to form the AP-1 complex, playing a crucial role in stress responses and inflammation regulation [40, 41]. It shows significant positive correlations with JUN and MYC (correlation coefficients of 0.91 and 0.84, respectively; $p < 0.05$), indicating a high level of functional similarity and suggesting a collaborative involvement in pathological processes of IgAN. FOS is enriched in pathways related to ribosomal function, MAPK signaling pathway, and ECM-receptor interactions, which are involved in protein synthesis, stress signal transduction, and the maintenance of renal structure [44]. In the model group, the expression of FOS is significantly reduced ($p < 0.05$), potentially influencing SGs assembly (which depends on ribosomal function) and inflammation balance by inhibiting these pathways. Changes in its expression can reflect the "stress-inflammation" state, providing a potential targets for intervention in IgAN [45, 46].

The MYC gene encodes the multifunctional transcription factor Myc, which regulates cell metabolism, proliferation, and stress adaptation, making it a core regulator of cellular homeostasis [47, 48]. It is strongly correlated with FOS($cor = 0.84$, $p < 0.001$), showing high functional similarity, and is enriched in pathways related to ribosomes, MAPK, and ECM-receptor interactions, participating in energy metabolism and stress responses [49]. The model group exhibited a significant reduction in MYC expression ($p < 0.001$), which may affect SGs formation by inhibiting ribosomal function, while also weakening the compensatory ability of cellular metabolism, exacerbating renal damage. Its significant downregulation makes it a highly specific key gene for the progression of IgAN, and targeting the restoration of MYC function may improve cellular stress adaptation and thereby alleviate renal pathological damage in IgAN [50, 51].

The ESR1 gene encodes estrogen receptor alpha, a key transcription factor that mediates estrogen signaling and is involved in cell metabolism, immune regulation, and tissue repair [52, 53]. In IgAN, ESR1 is enriched in pathways related to ribosomes, focal adhesions, and endocytosis, which are involved in protein synthesis, maintenance of renal structure, and cellular material transport [45]. Although ESR1 expression in the model group was slightly lower than that of the control group, the difference failed to achieve statistical significance, its extensive pathway associations—particularly its enrichment in ribosomal pathways—suggest that it may influence the formation of SGs by regulating ribosomal function (since SGs depend on the assembly of ribosome-associated RNA-binding proteins [10], thus participating in cellular stress adaptation. The expression trend of ESR1 provides clues for exploring the impact of ESR1-mediated, estrogen-related gender differences on IgAN susceptibility and may serve as a gender-specific intervention target [54].

As a key enzyme in prostaglandin synthesis, this enzyme plays a central role in inflammatory responses by catalyzing the production of pro-inflammatory prostaglandins, such as PGE2, from arachidonic acid

[55, 56]. In IgAN, PTGS2 is significantly enriched in the MAPK signaling pathway, ribosomes, and circadian rhythm pathways, closely related to inflammation activation, cellular stress, and metabolic rhythms [57]. The expression level of PTGS2 in the model group is notably decreased ($p < 0.05$), which may weaken inflammatory signaling by inhibiting the MAPK pathway [58, 59]. However, this reduction may also impair SGs-related compensatory mechanisms associated with stress, such as the protective effects mediated by prostaglandins in maintaining cellular stress tolerance [60]. Changes in its expression can reflect the "inflammation-stress" balance in IgAN, and targeting the precise regulation of PTGS2 may offer a new direction for IgAN treatment by suppressing excessive inflammation while maintaining cellular stress adaptation abilities.

In summary, these five genes form a synergistic network by cross-regulating pathways such as MAPK, ribosomal-related pathways, and ECM-receptor interactions: JUN and FOS primarily govern the "stress-inflammation-structure" regulation, MYC plays a central role in metabolism and stress adaptation, ESR1 relates to gender differences and SGs function, while PTGS2 mediates the balance between inflammation and metabolism. Their abnormal expression (with JUN, FOS, MYC, and PTGS2 being significantly downregulated and ESR1 showing a decreasing trend) may serve as combined indicators for assessing the progression of IgAN. Targeted interventions in their related pathways (such as activating JUN/FOS to modulate the MAPK pathway, or regulating PTGS2 activity) hold promise for restoring the balance of "stress adaptation-inflammation-structural stability", thereby offering a theoretical foundation for the accurate diagnosis and targeted treatment of SGs-associated IgAN.

The drug daidzein, identified through predictive screening, exhibited good binding activity in molecular docking with the proteins encoded by all five key genes (docking scores ranging from − 5 to -8.8 kcal/mol), particularly demonstrating stronger binding affinity with Esr1 and Ptgs2 (both at -8.7 kcal/mol). This result suggests that daidzeinmay achieve synergistic regulation of disease-related molecular pathways by simultaneously targeting multiple key genes, indicating its potential as a multi-target intervention drug. Additionally, the predictive analysis-derived screening results of 1,630 potential drugs provide a broad selection for further research, with daidzein's high ranking in Combined. Score and Odds. Ratio making it a priority candidate for validation. Further molecular dynamics simulations reveal the binding characteristics of daidzein with the proteins encoded by the key genes from a dynamic perspective. Regarding the binding stability and conformational flexibility of daidzein-protein complexes, the RMSD values of ESR1 and PTGS2 in complex with daidzein are low and exhibit rapid convergence, indicating a strong binding affinity and high conformational rigidity, which facilitates the formation of stable daidzein-protein complexes [61]. In contrast, FOS, JUN, and MYC undergo significant conformational adjustments during the early stages of the simulation; although they stabilize later, their RMSD values remain relatively high compared to those of ESR1 and PTGS2, indicating greater structural flexibility. This may be related to the functional characteristics of these proteins as transcription factors [62, 63]. From the perspective of structural dynamics and functional association, the binding of Ptgs2 with daidzein is the most stable, consistent with Ptgs2’s requirement to maintain a specific active conformation as an enzyme (COX-2) [64]. The flexible region of Esr1 is broader, which may relate to its mechanism of action as a nuclear receptor [65]. The high volatility at the N-terminus of FOS, JUN, and

MYC may be associated with the dynamic regulatory functions of their transcription activation domains [66]. Regarding the driving forces of binding, the number of hydrogen bonds between ESR1 and daidzein is significant and exhibits notable dynamic variation, indicating that hydrogen bonds are a key driving force in their interaction and that the binding mode has a degree of flexibility due to the notable dynamic variation in hydrogen bond numbers. In PTGS2, the core hydrogen bond framework is stable, suggesting that binding stability relies on fundamental hydrogen bonding interactions. Conversely, JUN and MYC contribute fewer hydrogen bonds and likely achieve binding with daidzein primarily through hydrophobic interactions and van der Waals forces, among other non-hydrogen bond interactions [67–69]. These differences provide molecular-level details for understanding the mechanism of action of daidzein and also offer a theoretical basis for subsequent optimization of daidzein's targeting through chemical modifications (such as enhancing the binding stability with FOS and JUN).

This study reveals potential molecular mechanisms related to SGs in IgAN, identifying key genes and signaling pathways, providing new evidence advance a more comprehensive theoretical understanding of IgAN pathogenesis, and filling a gap in the research field of IgAN-SGs. However, this study has certain limitations. First, the research based on the rat model has species differences compared to human IgAN, so the universality of gene expression needs to be validated in a larger clinical cohort. Second, the limited sample size may affect the statistical power. Furthermore, the causal relationship between the key genes regulating SG assembly and cell fate has not been directly confirmed through functional experiments. Additionally, the lack of protein level validation introduces uncertainty into the conclusions. Importantly, while molecular docking predicts that morin binds well with the target proteins, there is no experimental evidence to prove whether it can actually regulate the mRNA expression of key genes such as Jun and Fos in the IgAN model. Future research should expand the clinical sample size and integrate multi-omics data, using gene intervention techniques to clarify the causal mechanisms of key genes. Moreover, functional verification experiments for morin should be conducted—by administering it in cellular and animal models to directly detect its regulatory effects on key gene mRNA and protein expression, and linking this regulatory effect to kidney protection. This would provide a complete evidence chain for morin as a multi-target drug in the treatment of IgAN.

5. Conclusions

This study integrated transcriptomic data from a rat IgAN model with human stress granule-related genes to identify JUN, FOS, ESR1, PTGS2, and MYC as pivotal genes linking SGs to IgAN pathogenesis. These genes form a synergistic network, significantly enriched in crucial pathways such as MAPK signaling and ribosome function, suggesting their collective role in regulating cellular stress adaptation, immune-inflammatory responses, and extracellular matrix remodeling. The shared regulatory pattern by common transcription factors and non-coding RNAs further underscores their interconnected function. Molecular docking and dynamics simulations highlighted daidzein as a promising multi-target therapeutic candidate, demonstrating stable binding with the encoded proteins. Initial experimental validation supports the bioinformatics findings. These results advance our understanding of SG-related

mechanisms in IgAN and provide a foundational framework for developing novel diagnostic biomarkers and targeted therapeutic strategies.

Abbreviations

The following abbreviations are used in this manuscript:

SGs	Stress granules
IgAN	Immunoglobulin A nephropathy
DEGs	Differentially expressed genes
PPI	Protein-protein interaction
GO	Gene Ontology
KEGG	Kyoto Encyclopedia of Genes and Genomes
TFs	Transcription factors
miRNAs	microRNAs
lncRNAs	long non-coding RNAs
RT-qPCR	Reverse transcription-quantitative polymerase chain reaction
FC	FoldChange
FPKM	Fragments Per Kilobase of exon per Million mapped fragments
NES	Normalized Enrichment Score
GSVA	Gene Set Variation Analysis
RMSD	Root Mean Square Deviation
RMSF	Root Mean Square Fluctuation
GAPDH	Glyceraldehyde-3-Phosphate Dehydrogenase
AKI	Acute kidney injury
DN	Diabetic nephropathy
ESRD	End-stage renal disease
AP-1	Activator protein-1
Gd-IgA1	Galactose-deficient IgA1
PGE2	Prostaglandin E2
COX-2	Cyclooxygenase-2

Declarations

Ethics approval and consent to participate

The study was conducted in accordance with the revised Animals (Scientific Procedures) Act 1986 in the UK and Directive 2010/63/EU in Europe, and approved by the Ethics Committee of the First Affiliated Hospital of Xinjiang Medical University (protocol code IACUC-20230627-19, dated June 27, 2023).

Clinical trial number

Not applicable.

Consent for publication

Not applicable.

Data Availability Statement

The datasets generated and analysed during the current study are available in the NCBI repository,

[https://www.ncbi.nlm.nih.gov/bioproject/PRJNA1337934?reviewer=4bd0c1dtoqfgm3fff5ru9qm4ta]. BioProject: PRJNA1337934. The stress granule-related genes were obtained from the GeneCards database (https://www.genecards.org).

Competing interests

The authors declare no conflicts of interest.

Author Contributions

Conceptualization, methodology, writing-original draft preparation, writing-review and editing, Guzailinuer Sailaiajimu. Author has read and agreed to the published version of the manuscript.

Funding

This research was funded by the Natural Science Foundation of Xinjiang Uygur Autonomous Region, grant number 2025D01C424; the Health Commission of Xinjiang Uygur Autonomous Region, grant number BL202617.

Acknowledgments

We would like to express our sincere gratitude to all individuals and organizations who supported and assisted us throughout this research.. In conclusion, we extend our thanks to everyone who has supported and assisted us along the way. Without your support, this research would not have been possible.

References

1. Glassock RJ. An Expert Opinion on Current and Future Treatment Approaches in IgA Nephropathy. Adv Ther. 2025;42:2545-58.
2. Aseem S, Zheng S. Immunoglobulin A Nephropathy: A Review. Perm J. 2024;28:87-94.
3. Rajasekaran A, Julian BA, Rizk DV. IgA Nephropathy: An Interesting Autoimmune Kidney Disease. Am J Med Sci. 2021;361:176-94.
4. Filippone EJ, Gulati R, Farber JL. Contemporary review of IgA nephropathy. Front Immunol. 2024;15:1436923.
5. Girndt M. [Immunoglobulin A nephropathy-New treatment possibilities]. Inn Med (Heidelb). 2024;65:407-13.
6. El Karoui K, Fervenza FC, De Vriese AS. Treatment of IgA Nephropathy: A Rapidly Evolving Field. J Am Soc Nephrol. 2024;35:103-16.
7. Kim D, Wong MG. Corticosteroid Therapy in Immunoglobulin A Nephropathy: A Friend or Foe? Kidney Blood Press Res. 2023;48:392-404.
8. Yang C, Wang Z, Kang Y, Yi Q, Wang T, Bai Y, et al. Stress granule homeostasis is modulated by TRIM21-mediated ubiquitination of G3BP1 and autophagy-dependent elimination of stress granules. Autophagy. 2023;19:1934-51.
9. Redding A, Grabocka E. Stress granules and hormetic adaptation of cancer. Trends Cancer. 2023;9:995-1005.
10. Zhu J, Su H. Assembly and disassembly of stress granules in kidney diseases. iScience. 2025;28:112578.
11. Yang W, Zhang M, Li J, Qu S, Zhou F, Liu M, et al. YTHDF1 mitigates acute kidney injury via safeguarding m(6)A-methylated mRNAs in stress granules of renal tubules. Redox Biol. 2023;67:102921.
12. Liu Z, Zhao E, Li H, Lin D, Huang C, Zhou Y, et al. Identification and validation of a novel stress granules-related prognostic model in colorectal cancer. Front Genet. 2023;14:1105368.
13. Liu S, Wang Z, Zhu R, Wang F, Cheng Y, Liu Y. Three Differential Expression Analysis Methods for RNA Sequencing: limma, EdgeR, DESeq2. J Vis Exp. 2021.
14. Wang J, Wu N, Feng X, Liang Y, Huang M, Li W, et al. PROS1 shapes the immune-suppressive tumor microenvironment and predicts poor prognosis in glioma. Front Immunol. 2022;13:1052692.
15. Gu Z. Complex heatmap visualization. Imeta. 2022;1:e43.
16. Paparozzi V, Nardini C. tidysbml: R/Bioconductor package for SBML extraction into dataframes. Bioinform Adv. 2024;4:vbae148.
17. Zhou W, Li H, Zhang J, Liu C, Liu D, Chen X, et al. Identification and mechanism analysis of biomarkers related to butyrate metabolism in COVID-19 patients. Ann Med. 2025;57:2477301.

18. Suo Z, Yang J, Zhou B, Qu Y, Xu W, Li M, et al. Whole-transcriptome sequencing identifies neuroinflammation, metabolism and blood-brain barrier related processes in the hippocampus of aged mice during perioperative period. CNS Neurosci Ther. 2022;28:1576-95.
19. Huang S. Efficient analysis of toxicity and mechanisms of environmental pollutants with network toxicology and molecular docking strategy: Acetyl tributyl citrate as an example. Sci Total Environ. 2023;905:167904.
20. Wang N, Song M, Gu H, Gao Y, Yu G, Lv F, et al. A Factor Analysis Model for Rapid Evaluation of the Semen Quality of Fertile Men in China. J Multidiscip Healthc. 2022;15:431-41.
21. Hänzelmann S, Castelo R, Guinney J. GSVA: gene set variation analysis for microarray and RNA-seq data. BMC Bioinformatics. 2013;14:7.
22. Yan L, Han X, Zhang M, Fu Y, Yang F, Li Q, et al. Integrative analysis of TBI data reveals Lgmn as a key player in immune cell-mediated ferroptosis. BMC Genomics. 2023;24:747.
23. Yu G. Gene Ontology Semantic Similarity Analysis Using GOSemSim. Methods Mol Biol. 2020;2117:207-15.
24. Bokaii Hosseini Z, Rajabi F, Morovatshoar R, Ashrafpour M, Behboodi P, Zareie D, et al. Downregulation of LPAR1 Promotes Invasive Behavior in Papillary Thyroid Carcinoma Cells. Cancer Inform. 2024;23:11769351241277012.
25. Xie Z, Bailey A, Kuleshov MV, Clarke DJB, Evangelista JE, Jenkins SL, et al. Gene Set Knowledge Discovery with Enrichr. Curr Protoc. 2021;1:e90.
26. Yu D, Li H, Liu Y, Yang X, Yang W, Fu Y, et al. Application of the molecular dynamics simulation GROMACS in food science. Food Res Int. 2024;190:114653.
27. Mitteer DR, Greer BD, Randall KR, Briggs AM. Further Evaluation of Teaching Behavior Technicians to Input Data and Graph Using GraphPad Prism. Behav Anal (Wash D C). 2020;20:81-93.
28. Zhou X, Wang N, Zhang Y, Yu P. Expression of CCL2, FOS, and JUN May Help to Distinguish Patients With IgA Nephropathy From Healthy Controls. Front Physiol. 2022;13:840890.
29. Noor F, Saleem MH, Aslam MF, Ahmad A, Aslam S. Construction of miRNA-mRNA network for the identification of key biological markers and their associated pathways in IgA nephropathy by employing the integrated bioinformatics analysis. Saudi J Biol Sci. 2021;28:4938-45.
30. Wang S, Kwon SH, Su Y, Dong Z. Stress granules are formed in renal proximal tubular cells during metabolic stress and ischemic injury for cell survival. Am J Physiol Renal Physiol. 2019;317:F116-f23.
31. Stamellou E, Seikrit C, Tang SCW, Boor P, Tesař V, Floege J, et al. IgA nephropathy. Nat Rev Dis Primers. 2023;9:67.
32. Fonteneau G, Redding A, Hoag-Lee H, Sim ES, Heinrich S, Gaida MM, et al. Stress Granules Determine the Development of Obesity-Associated Pancreatic Cancer. Cancer Discov. 2022;12:1984-2005.

33. Coppo R, Camilla R, Amore A, Peruzzi L. Oxidative stress in IgA nephropathy. Nephron Clin Pract. 2010;116:c196-8, discussion c9.
34. Frąk W, Dąbek B, Balcerczyk-Lis M, Motor J, Radzioch E, Młynarska E, et al. Role of Uremic Toxins, Oxidative Stress, and Renal Fibrosis in Chronic Kidney Disease. Antioxidants (Basel). 2024;13.
35. Suzuki H, Novak J. IgA glycosylation and immune complex formation in IgAN. Semin Immunopathol. 2021;43:669-78.
36. Zhang J, Shen M. The Role of IL-17 in Systemic Autoinflammatory Diseases: Mechanisms and Therapeutic Perspectives. Clin Rev Allergy Immunol. 2025;68:27.
37. Zhang T, Huo H, Zhang Y, Tao J, Yang J, Rong X, et al. Th17 cells: A new target in kidney disease research. Int Rev Immunol. 2024;43:263-79.
38. Zhao S, Li R, Xia Y, Wang X, Liu Z, Chu Q, et al. Targeting ECM-producing cells with CAR-T therapy alleviates fibrosis in chronic kidney disease. Cell Stem Cell. 2025;32:1390-402.e9.
39. Lin H, Ye Z, Xu R, Li XE, Sun B. The transcription factor JUN is a major regulator of quiescent pancreatic stellate cell maintenance. Gene. 2023;851:147000.
40. Seo H, González-Avalos E, Zhang W, Ramchandani P, Yang C, Lio CJ, et al. BATF and IRF4 cooperate to counter exhaustion in tumor-infiltrating CAR T cells. Nat Immunol. 2021;22:983-95.
41. Choi Y, Jeon H, Akin JW, Curry TE, Jo M. The FOS/AP-1 Regulates Metabolic Changes and Cholesterol Synthesis in Human Periovulatory Granulosa Cells. Endocrinology. 2021;162.
42. Anguita-Ruiz A, Bustos-Aibar M, Plaza-Díaz J, Mendez-Gutierrez A, Alcalá-Fdez J, Aguilera CM, et al. Omics Approaches in Adipose Tissue and Skeletal Muscle Addressing the Role of Extracellular Matrix in Obesity and Metabolic Dysfunction. Int J Mol Sci. 2021;22.
43. Nagesh R, Kiran Kumar KM, Naveen Kumar M, Patil RH, Sharma SC. Regulation of Jun and Fos AP-1 transcription factors by JNK MAPKs signaling cascade in areca nut extract treated KB cells. Biochem Biophys Rep. 2021;27:101090.
44. Zhao H, Dinh TH, Wang Y, Yang Y. The roles of MAPK signaling pathway in ovarian folliculogenesis. J Ovarian Res. 2025;18:152.
45. Chen C, He Y, Ni Y, Tang Z, Zhang W. Identification of crosstalk genes relating to ECM-receptor interaction genes in MASH and DN using bioinformatics and machine learning. J Cell Mol Med. 2024;28:e18156.
46. Babaei P, Faraji N, Eyvani KJGE. c-Fos Expression Differentially Acts in the Healthy Brain Compared with Alzheimer’s Disease. 2025 0-.
47. Doha ZO, Sears RC. Unraveling MYC's Role in Orchestrating Tumor Intrinsic and Tumor Microenvironment Interactions Driving Tumorigenesis and Drug Resistance. Pathophysiology. 2023;30:400-19.
48. Boyack I, Berlied A, Peterson C. A Potential Role for c-MYC in the Regulation of Meibocyte Cell Stress. Cells. 2025;14.

49. Kumar D, Kanchan R, Chaturvedi NK. Targeting protein synthesis pathways in MYC-amplified medulloblastoma. Discov Oncol. 2025;16:23.
50. Shu J, Li H, Li H. Identification and Validation of Aging-Related Genes in IgA Nephropathy in the Asian Population. Int J Gen Med. 2025;18:3851-70.
51. Alimohammadi M, Kahkesh S, Abbasi A, Hashemi M, Khoshnazar SM, Taheriazam A, et al. LncRNAs and IgA nephropathy: underlying molecular pathways and clinical applications. Clin Exp Med. 2025;25:140.
52. Chen P, Li B, Ou-Yang L. Role of estrogen receptors in health and disease. Front Endocrinol (Lausanne). 2022;13:839005.
53. O'Brien MH, Pitot HC, Chung SH, Lambert PF, Drinkwater NR, Bilger A. Estrogen Receptor-α Suppresses Liver Carcinogenesis and Establishes Sex-Specific Gene Expression. Cancers (Basel). 2021;13.
54. Deng W, Tan X, Zhou Q, Ai Z, Liu W, Chen W, et al. Gender-related differences in clinicopathological characteristics and renal outcomes of Chinese patients with IgA nephropathy. BMC Nephrol. 2018;19:31.
55. Saindane M, Rallabandi HR, Park KS, Heil A, Nam SE, Yoo YB, et al. Prognostic Significance of Prostaglandin-Endoperoxide Synthase-2 Expressions in Human Breast Carcinoma: A Multiomic Approach. Cancer Inform. 2020;19:1176935120969696.
56. Kamal MV, Damerla RR, Dikhit PS, Kumar NA. Prostaglandin-endoperoxide synthase 2 (PTGS2) gene expression and its association with genes regulating the VEGF signaling pathway in head and neck squamous cell carcinoma. J Oral Biol Craniofac Res. 2023;13:567-74.
57. Huang L, Zuo Y, Yang H, He X, Zhang L. Identification of key genes as potential diagnostic and therapeutic targets for comorbidity of myasthenia gravis and COVID-19. Front Neurol. 2023;14:1334131.
58. Li X, Tang H, Tang Q, Chen W. Decoding the Mechanism of Huanglian Jiedu Decoction in Treating Pneumonia Based on Network Pharmacology and Molecular Docking. Front Cell Dev Biol. 2021;9:638366.
59. Gusson-Zanetoni JP, Cardoso LP, de Sousa SO, de Melo Moreira Silva LL, de Oliveira Martinho J, Henrique T, et al. Molecular Aspects of Piperine in Signaling Pathways Associated with Inflammation in Head and Neck Cancer. Int J Mol Sci. 2024;25.
60. Finetti F, Travelli C, Ercoli J, Colombo G, Buoso E, Trabalzini L. Prostaglandin E2 and Cancer: Insight into Tumor Progression and Immunity. Biology (Basel). 2020;9.
61. Mizuno-Yasuhira A, Nakai Y, Gunji E, Uchida S, Takahashi T, Kinoshita K, et al. A Strategy for assessing potential drug-drug interactions of a concomitant agent against a drug absorbed via an intestinal transporter in humans. Drug Metab Dispos. 2014;42:1456-65.
62. Beaulieu ME, Castillo F, Soucek L. Structural and Biophysical Insights into the Function of the Intrinsically Disordered Myc Oncoprotein. Cells. 2020;9.

63. Shah K, Ansari M, Saeed S, Wali A, Mushtaq Yasinzai M. Nilotinib: Disrupting the MYC-MAX Heterocomplex. Bioinform Biol Insights. 2024;18:11779322241267056.
64. Pandaleke TA, Handono K, Widasmara D, Susianti H. The immunomodulatory activity of Orthosiphon aristatus against atopic dermatitis: Evidence-based on network pharmacology and molecular simulations. J Taibah Univ Med Sci. 2024;19:164-74.
65. Saha T, Lukong KE. Decoding estrogen receptor and GPER biology: structural insights and therapeutic advances in ERα-positive breast cancer. Front Oncol. 2025;15:1513225.
66. Yang J, Chung CI, Koach J, Liu H, Navalkar A, He H, et al. MYC phase separation selectively modulates the transcriptome. Nat Struct Mol Biol. 2024;31:1567-79.
67. Lekmine S, Benslama O, Kadi K, Brik A, Djeffali O, Ounissi M, et al. Preliminary Investigation of Astragalus arpilobus subsp. hauarensis: LC-MS/MS Chemical Profiling, In Vitro Evaluation of Antioxidant, Anti-Inflammatory Properties, Cytotoxicity, and In Silico Analysis against COX-2. Antioxidants (Basel). 2024;13.
68. Bonet LFS, Loureiro JP, Pereira GRC, Da Silva ANR, De Mesquita JF. Molecular dynamics and protein frustration analysis of human fused in Sarcoma protein variants in Amyotrophic Lateral Sclerosis type 6: An In Silico approach. PLoS One. 2021;16:e0258061.
69. Kaur M, Kaur B, Kaur J, Kaur A, Bhatti R, Singh P. Role of water in cyclooxygenase catalysis and design of anti-inflammatory agents targeting two sites of the enzyme. Sci Rep. 2020;10:10764.

Figures

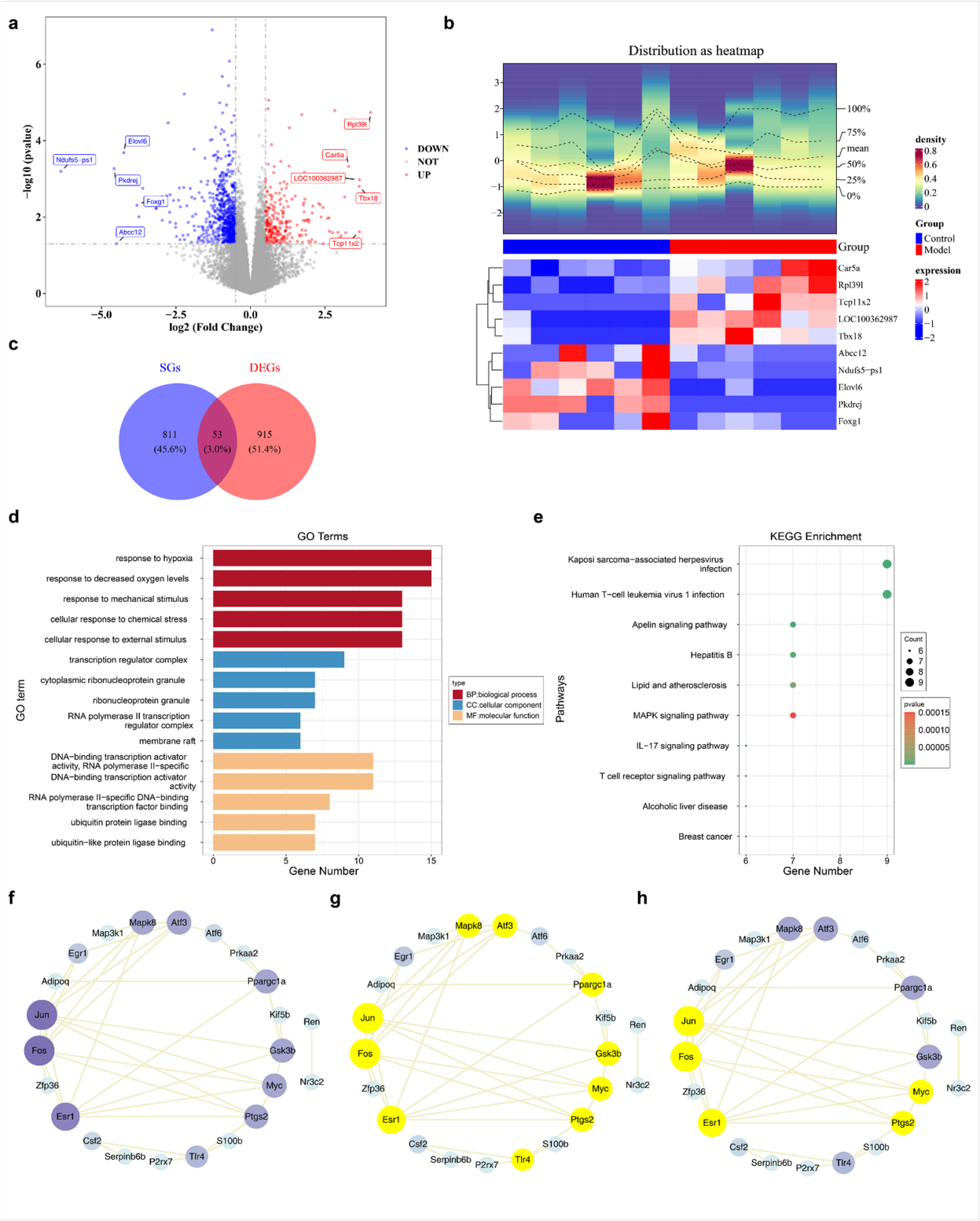


Figure 1

Identification of key genes related to SGs in IgAN. (a) Volcano plot of DEGs between the rat IgAN model group and the control group. Red dots represent upregulated genes, blue dots represent downregulated genes, and gray dots represent genes with no significant difference. (b) Heatmap of DEGs. The upper part is a density heatmap of expression levels, where a redder color indicates a higher expression density. The lower part is an expression heatmap, where pink represents high expression and blue

represents low expression; in terms of grouping, red represents the IgAN model group and blue represents the control group. (c) Venn diagram of the intersection between SGs-RGs and DEGs. (d) GO enrichment analysis of candidate genes. In the figure, red represents BP, blue represents CC, and yellow represents MF; a longer bar indicates a greater number of enriched genes. (e) KEGG enrichment analysis of candidate genes. In the figure, a larger dot indicates a greater number of enriched genes, and a greener color indicates higher significance. (f) PPI network of candidate genes. Circles represent proteins encoded by each candidate gene, and lines represent interaction links between proteins. According to the increase in Degree value from small to large, the dots of each gene increase in size, and the color gradually changes from light blue to dark purple. (g) PPI network of the top 10 candidate genes ranked by Degree. The top 10 genes are highlighted in yellow. (h) PPI network of key sub-modules screened by MCODE. Key genes are highlighted in yellow.Abbreviations: SGs, Stress Granules; IgAN, Immunoglobulin A Nephropathy; DEGs, Differentially Expressed Genes; SGs-RGs, Stress Granules-Related Genes; GO, Gene Ontology; BP, Biological Process; CC, Cellular Component; MF, Molecular Function; KEGG, Kyoto Encyclopedia of Genes and Genomes; PPI, Protein-Protein Interaction; MCODE, Molecular Complex Detection; Degree, a metric used to measure the number of connections a node has in a network.

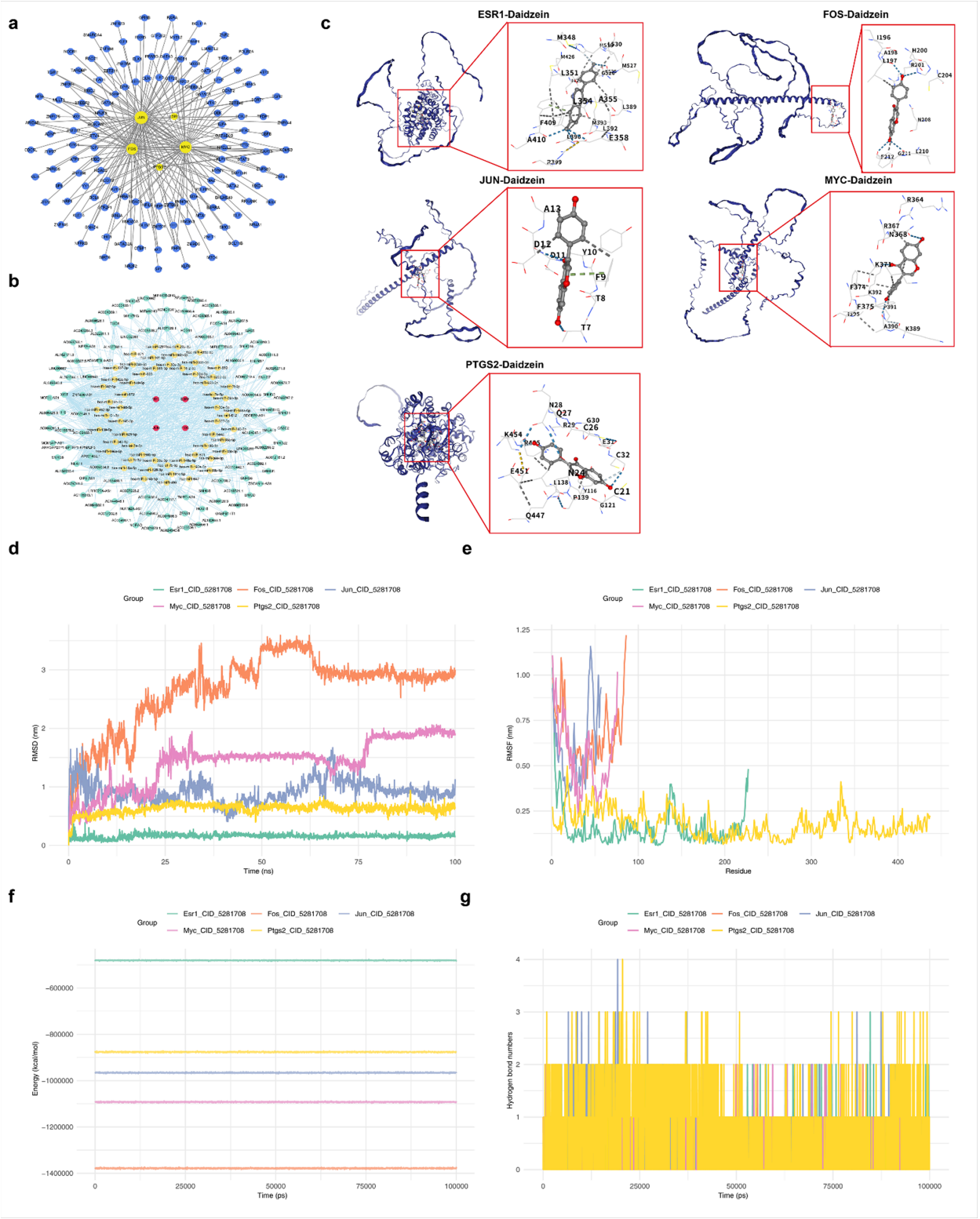


Figure 2

Molecular regulation, drug prediction, molecular docking, and molecular dynamics simulation of key genes. (a) TF-mRNA regulatory network. Yellow circles represent key genes (mRNA), and blue circles represent TFs. (b) lncRNA-miRNA-mRNA regulatory network. Red circles represent key genes (mRNA), yellow circles represent miRNAs, and green circles represent lncRNAs. (c) Molecular docking of proteins encoded by key genes with the drug daidzein. The left part shows the docking sites between proteins

encoded by key genes and drug molecules, and the 3D structure on the right shows the chemical structure of morin. (d) RMSD curves of molecular dynamics simulations. (e) RMSF curves of molecular dynamics simulations. (f) Protein energy change curves of molecular dynamics simulations. (g) Hydrogen bond number change curves of molecular dynamics simulations. In Figures (d-g), lines of different colors represent different key genes.Abbreviations: TF, Transcription Factor; lncRNA, Long Non-Coding Ribonucleic Acid; miRNA, Micro Ribonucleic Acid; RMSD, Root Mean Square Deviation; RMSF, Root Mean Square Fluctuation

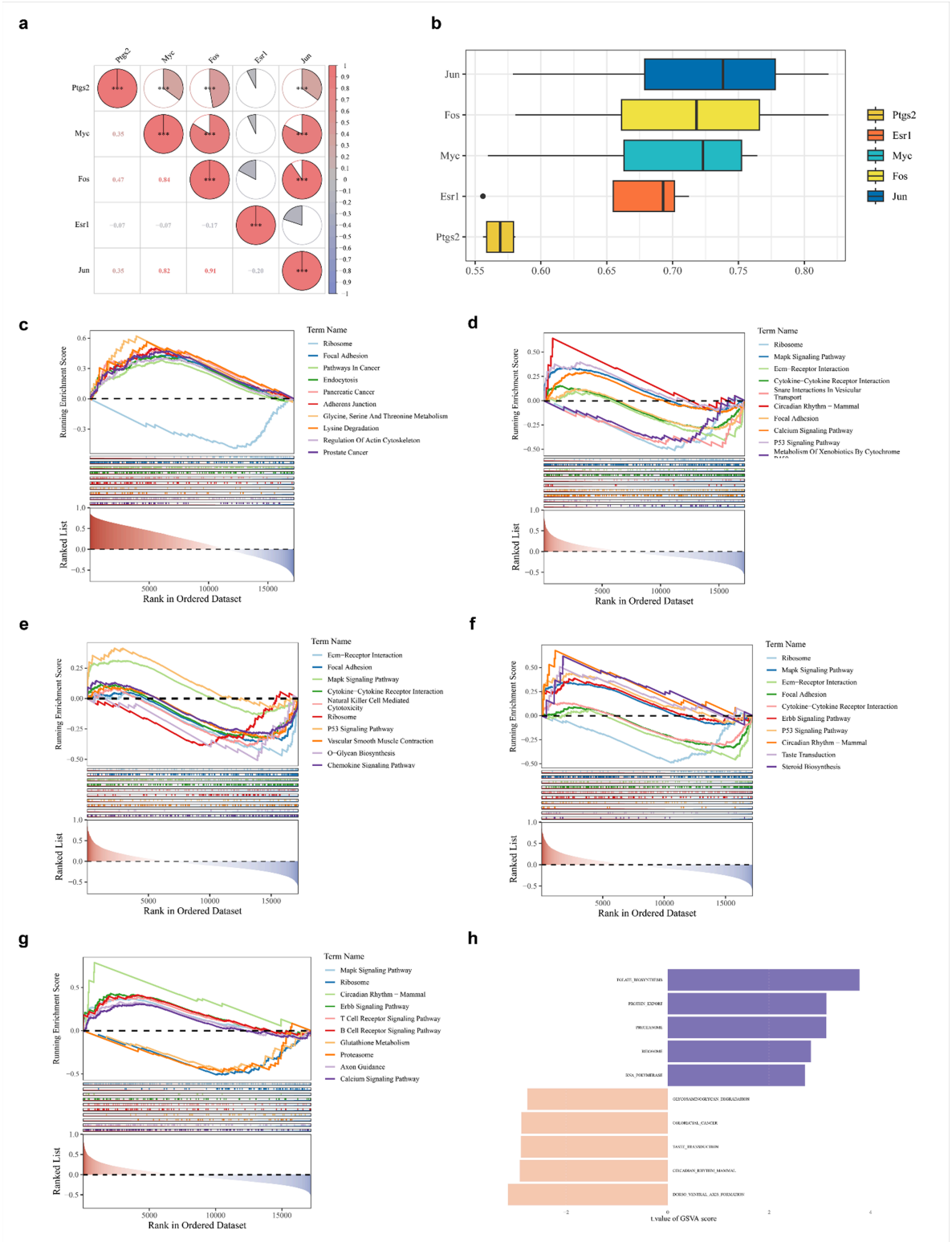


Figure 3

Correlation, functional similarity, and pathway enrichment analysis of key genes. (a) Correlation heatmap between key genes. The redder the color, the stronger the positive correlation; the bluer the color, the stronger the negative correlation. ***p < 0.001. (b) Functional similarity analysis of key genes. The ordinate and different colors represent the 5 key genes, and the abscissa represents the functional similarity score. (c-g) GSEA plots of Esr1 (c), Fos (d), Jun (e), Myc (f), and Ptgs2 (g) genes. The upper part of each plot is an enrichment score line chart, where each line represents a pathway and the peak of each line is the enrichment score of that pathway. The genes before the peak are the core genes of the pathway gene set; a peak in the upper left indicates the core genes are mainly upregulated, while a peak in the lower right indicates the core genes are mainly downregulated. The middle part marks the genes in the gene set with short lines, and the lower part shows the rank value distribution of genes. (h) GSVA of the IgAN model group and the control group. Purple represents the upregulated gene sets, and orange represents the downregulated gene sets.Abbreviations: GSEA, Gene Set Enrichment Analysis; GSVA, Gene Set Variation Analysis; IgAN, Immunoglobulin A Nephropathy

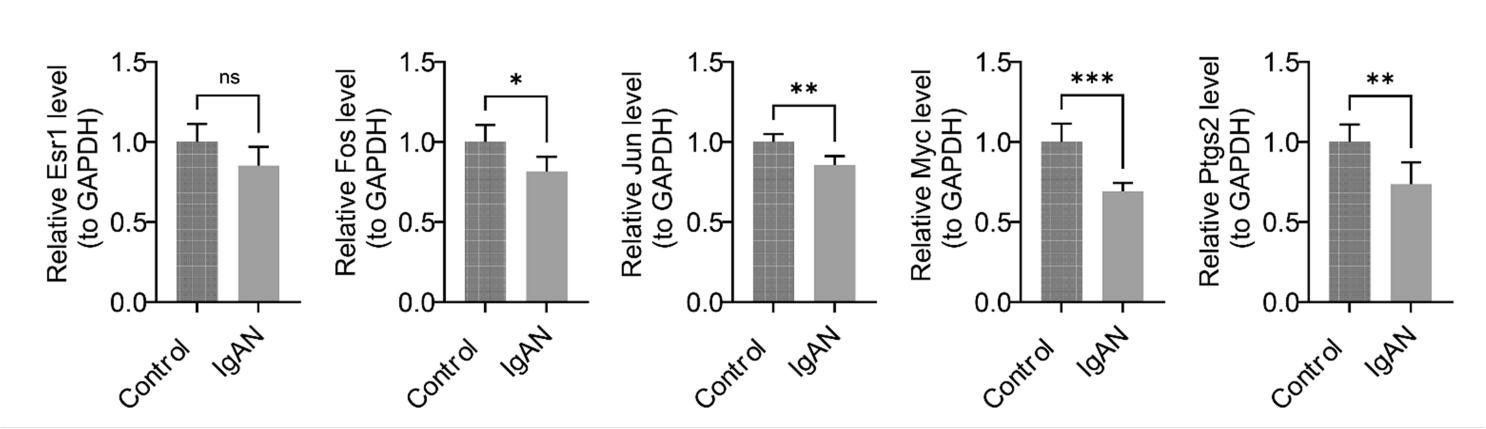


Figure 4

RT-qPCR validation of 5 key genes (Jun, Fos, Ptgs2, Myc, Esr1). The figure shows the relative expression levels of 5 key genes in the control group and the IgAN model group. *p < 0.05, **p < 0.01, ***p < 0.001, and ns indicates no significance. Abbreviations: RT-qPCR, Reverse Transcription-Quantitative Polymerase Chain Reaction; IgAN, Immunoglobulin A Nephropathy; ns, no significance

Supplementary Files

This is a list of supplementary files associated with this preprint. Click to download.

- Additionalfile1.xlsx
- Additionalfile2.xlsx
- Additionalfile3.xlsx

- Additionalfile4.xlsx
- Additionalfile5.xlsx
- Additionalfile6.xlsx
- Additionalfile7.xlsx
- Additionalfile8.xlsx
- Additionalfile9.xlsx
- Additionalfile10.xlsx
- Additionalfile11.xlsx
- Additionalfile12.xlsx
- Additionalfile13.xlsx
- Additionalfile14.xlsx
- Additionalfile15.xlsx